Ultrathin Atomic-Layer-Deposited In_2O_3 Radio-Frequency Transistors with Record High f_T of 36 GHz and BEOL Compatibility

Dongqi Zheng†, Adam Charnas†, Jian-Yu Lin, Jackson Anderson, Dana Weinstein and Peide D. Ye*
Elmore Family School of Electrical and Computer Engineering, Purdue University, West Lafayette, IN 47907, USA
†These authors contributed equally to this work. *Email: yep@purdue.edu

Abstract

In this work, we report back-end-of-line (BEOL) compatible In_2O_3 RF transistors with cut-off frequencies (f_T) up to 36 GHz, which is the highest among all metal oxide semiconductor channel RF transistors to date. Due to the outstanding transport properties and high scalability of In_2O_3, record-high f_T value can be achieved with V_{DS} at 0.8 V and V_{GS} at -0.8 V on 2-nm thick, 40 nm-long channel devices. This work demonstrates the first ever BEOL oxide RF transistor with mm-Wave band operation frequency. In addition to improve the performance at Si CMOS clock frequencies for 3D integrated circuits (IC), it also offers the possibility for potential applications in future energy-efficient 6G wireless communication devices.

Introduction

Oxide semiconductors have been explored as promising channel materials for BEOL logic and memory transistor applications toward monolithic 3D integration [1-4]. Recently, ALD-grown In_2O_3 has emerged as a favorable candidate due to its disorder-resistant high carrier density, high mobility, and ultra-low contact resistivity from its unique charge neutrality level (CNL) band alignment and intrinsic high electron band-velocity at high electron density [5,6]. Tremendous effort has been put into material innovation and device optimization of In_2O_3 resulting in record on-state performance of 10-20 A/mm on-current and 4 S/mm transconductance [6,7]. As an amorphous oxide, In_2O_3 devices can be fabricated on a low thermal budget making them especially suited for BEOL applications. Transistors with channels as thin as 0.5 nm have been reported [1], and the electron mobility can reach over 100 $cm^2/V{\cdot}s$ [8] with near-ideal subthreshold swing, engineerable V_T, and excellent scalability. However, oxide semiconductor RF transistors, especially devices with extremely high operation frequency, are still under-developed, and improvement to figures of merit of such devices is also power-hungry, relying on large bias voltages [9-11]. In this work, by leveraging the unique features of high-performance In_2O_3 channel and optimized device structure, we successfully achieve a 2-nm-thick, 40-nm-long, In_2O_3-based RF transistor with an extremely high cut-off frequency of 36 GHz, in the mm-wave band. The maximum oscillation frequency (f_{max}) reaches 5.2 GHz in the device with 40-nm channel and can be further improved to 9.5 GHz in longer channel devices (240 nm).

Experiments

The fabrication process flow is illustrated in Fig.1. The substrate is highly resistive intrinsic silicon (>10 kΩ/□) with 300 nm SiO_2 for reduced substrate parasitics at high frequencies. A bilayer lithography process was used to avoid jagged metal edges, followed by an e-beam evaporated 3 nm Ti/80 nm Au/17 nm Ni bottom gate stack for lower gate resistance. 5 nm HfO_2 was grown by ALD at 200 °C for the gate dielectric layer. Then, an ultra-thin 2 nm layer of In_2O_3 channel layer was deposited by ALD at 225 °C. The thickness of ALD In_2O_3 was determined by ellipsometry (Gaertner L116A) calibrated by HRTEM and AFM [5]. Channel isolation and gate window openings were done simultaneously by photolithography and BCl_3/Ar plasma dry etching. The source and drain contacts were defined by e-beam lithography and e-beam evaporation of 60 nm Ni, followed by large contact pads consisting of a thicker 100 nm Ni/200 nm Au. The final device schematic is shown in Fig. 2. Electrical characterization was performed with a Keysight B1500 system and RF characteristics were measured using a Keysight N5225A vector network analyzer (VNA) from 30 MHz to 20 GHz. DC biases were provided by Keithley 2400 SMUs connected to the VNA bias tees and synchronized programmatically. On-wafer short and open device structures were fabricated and characterized at the same time to de-embed pad parasitic effects.

Results and Discussion

C-V measurement of the 5 nm ALD HfO_2 dielectric is shown in Fig. 3, exhibiting a highly scaled EOT of 2.1 nm. The as-fabricated device array is presented in Fig. 4, and false-color SEM of a fabricated device in the red selection is shown in Fig. 5, with a zoom-in view of the functional transistor region. DC measurement was carried out first to identify optimal biasing points. Well-behaved saturation can be observed in the long-channel devices (L_{CH} = 1 μm) with an I_D of 300 mA/mm at V_{DS} of 3 V and V_{GS} of 3 V. The transfer curve of the same device is shown in Fig. 7, where well-controlled on and off performance is shown with an on-off ratio of over 10^{10}. Behaviors of 40 nm short channel device performance are presented in Figs. 8-9. A significant high current of 750 mA/mm can be achieved with a very small drive voltage of 0.3 V due to the high carrier density and mobility. It is also notable that limited on-off ratio of 10^4 is impacted by gate leakage due to the large negative threshold voltage. V_T can be shifted to positive with O_2 annealing or plasma treatment. The de-embedded S parameters of an example 40 nm device are shown Figs. 10-12. Our de-embedding method only removes the GSG pad parasitics, so the difference from before de-embedding is minor as reported earlier [11]. Systematic investigation of V_{DS} dependent f_T with V_{GS} fixed at -0.8 V is illustrated in Fig. 13 to validate the biasing. Self-heating effects start to kick in when the drive voltage is over 0.8 V, resulting in a decreasing trend after f_T peaks at 36 GHz. This phenomenon can be tackled by thermal engineering and effective doping [4, 12]. Fig. 14 shows the extraction of f_T from the device with the highest value among the measured devices (L_{CH} = 40 nm). A f_T of 36 GHz is achieved with V_{GS} and V_{DS} as small as -0.8 V and 0.8 V, respectively. Maximum oscillation frequency (f_{max}) was extracted from Mason's unilateral gain (U) in Fig. 15. Here, the gate length (L_G) is fixed at 40 nm, and channel length is swept by increasing underlap (L_{UN}) between S/D and gate. As a result, 40-nm-long channel shows a f_{max} of 5.7 GHz, and longer channel of 240 nm can improve to be 9.7 GHz due to larger output resistance from the better saturation and optimized parasitics. With channel length scaling, an increasing trend of f_T can be observed in Fig. 16 as the g_m significantly increased. There is plenty room for further improvement with the help of novel patterning techniques [9]. A benchmark plot of f_T vs. channel length is shown in Fig. 17 that compares the performance of all reported metal oxide thin-film RF transistors. This work marks the highest value of 36 GHz, entering the mm-wave range. Detailed information such as biasing voltage, device parameters and figure of merits of state-of-the-art BEOL-compatible device performance is further summarized in Table 1, where this In_2O_3 work outperforms with thinnest film, smallest bias voltage/power consumption, and highest operation frequency.

Conclusion

In summary, a record-high f_T of 36 GHz was achieved by employing 2-nm-thick, 40-nm-long ALD-grown In_2O_3 channel RF transistors. The biasing voltage of V_{DS} and V_{GS} are only 0.8 V and -0.8 V, which is helpful toward energy-efficient RF devices. This work also provides a clear route for the potential of applying BEOL oxide semiconductor devices for 6G wireless communication applications. The work is supported by AFOSR, SRC nCore IMPACT Center, and DARPA/SRC JUMP ASCENT Center.

Reference: [1] M. Si et al., Nat. Electron., p.164, 2022. [2] S. Li et al., IEDM, p. 40.5.1. 2020. [3] W. Chakraborty et al., IEEE TED, p. 5336, 2020. [4] D. Zheng et al., IEDM, p. 4.3.1, 2022. [5] M. Si et al., Nano Lett., p.500, 2022 [6] Z. Lin et al., ACS Nano, p.21536 2020. [7] Z. Zhang et al., IEEE EDL, p.1905, 2022. [8] M. Si, et al., VLSI, TF 2-4, 2021. [9] C. Wang et al., VLSI, p. 294, 2022. [10] B. Bayraktaroglu et al., IEEE EDL, p. 946, 2009. [11] A. Charnas et al., IEEE TED, p.532, 2023. [12] P.-Y. Liao, VLSI, T5-2, 2022 [13] Y.-L. Wang et al., ECS Trans., p. 23, 2007. [14] N. Münzenrieder et al., Flex. Print. Electron., p. 015007, 2020. [15] Y. Wang et al., IEEE TED, p. 1377, 2018. [16] N. Münzenrieder et al., IEEE TED, p. 2815, 2013. [17] C. Tückmantel et al., IEEE EDL, p. 1786, 2020. [18] L.-Y. Su et al., Solid-State Elect., p. 122, 2015. [19] Li, S. et al., Nat. Mater., p. 1091, 2019. [20] M. Wang et al., IEDM, p. 8.2.1-2019. [21] Y. Mehlman et al., DRC, p. 1-2, 2017.

❑High-resistivity intrinsic silicon (>10kΩ/□) substrate cleaning
❑E-beam evaporation of 3 nm Ti/80 nm Au/17 nm Ni as buried gate
❑ALD growth of 5 nm HfO_2 at 200°C as dielectric
❑ALD growth of 2 nm In_2O_3 at 225°C
❑Isolation through Ar/BCl_3 dry etch E-beam evaporation of 60 nm Ni as Source/Drain
❑E-beam evaporation of Ni/Au as large pads

Fig. 1. Fabrication process flow of In_2O_3 RF transistors with scaled channel and optimized gate stack.

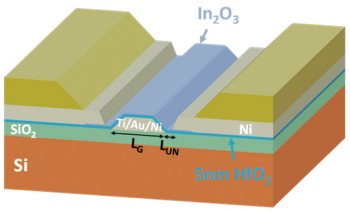

Fig. 2. Schematic diagram of a functional BEOL-compatible In_2O_3 transistor (L_{UN} indicates the underlap between gate and S/D, $L_{CH} = L_G + 2 \cdot L_{UN}$).

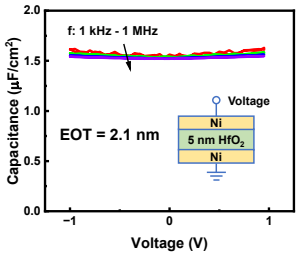

Fig. 3. C-V characterization of 5 nm ALD HfO_2 with an EOT of 2.1 nm.

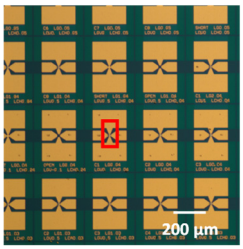

Fig. 4. Optical image of as-fabricated In_2O_3 RF transistors array.

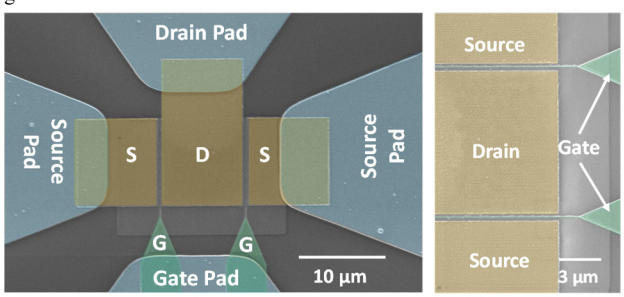

Fig. 5 False-color SEM image of GSG RF structure as zoomed in Fig. 4.

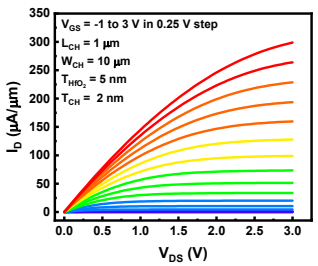

Fig. 6. Output characteristics of a long-channel transistor, where the current is well saturated at high V_{DS}.

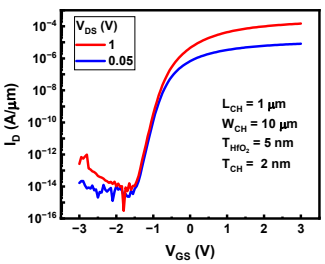

Fig. 7. Transfer curves of the same device in Fig. 6, showing well-controlled off-state performance with high on/off ratio.

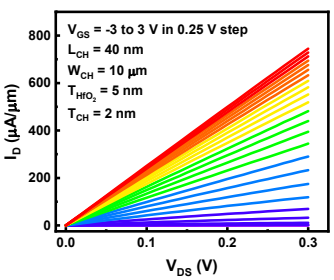

Fig. 8. Output curves of a scaled short-channel transistor with L_{CH} = 40 nm showing a current of 745 μA/μm at V_{DS} = 0.3 V and V_{GS} = 3 V.

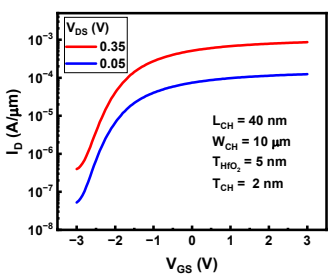

Fig. 9. I_{DS}-V_{GS} output curves of the same device in Fig. 8, limited on-off ratio is due to the very negative V_{TH}.

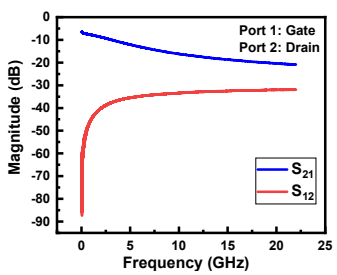

Fig. 10. Measured S parameters (S_{12} and S_{21}) of an example 40-nm-channel-length RF transistor.

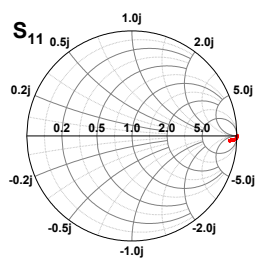

Fig. 11. Measured S_{11} of an example 40-nm-channel-length RF transistor.

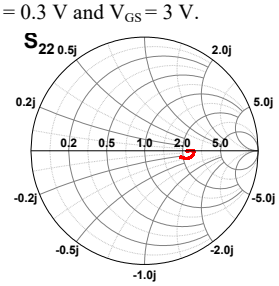

Fig. 12. Measured S_{22} of an example 40-nm-channel-length RF transistor.

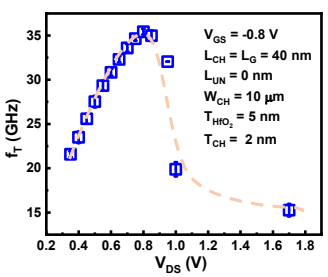

Fig. 13. V_{DS}-dependent f_T with V_{GS} biased at -0.8V, each point is extracted from at least five devices.

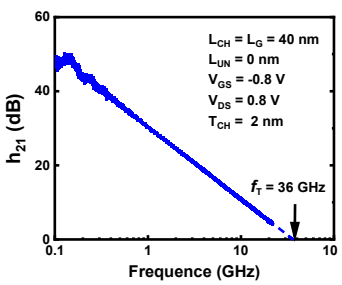

Fig. 14. Extraction of f_T the device with the highest among the measured devices; V_{GS} and V_{DS} are -0.8 V and 0.8 V, respectively.

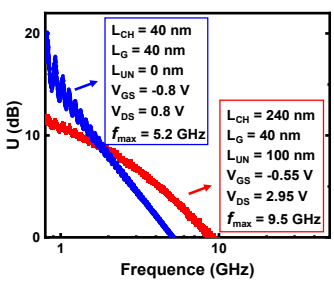

Fig. 15. Extracted f_{max} of 5.2 GHz and 9.5 GHz for the devices with channel length of 40 nm (V_{DS} = 0.8 V) and 240 nm (V_{DS} = 2.95 V).

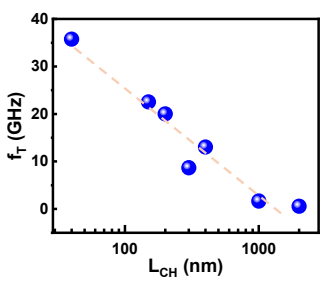

Fig. 16. Channel length dependent f_T showing an increasing trend with channel length scaled.

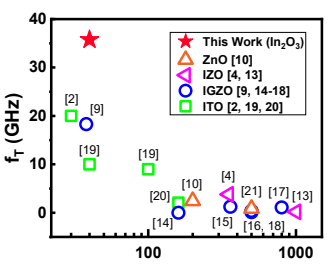

Fig. 17. Benchmark plot of f_T vs L_{CH} among all represented oxide semiconductor channel transistors.

Material	T_{CH} (nm)	L_{CH} (nm)	V_{GS} (V)	V_{DS} (V)	f_T (GHz)	Ref
In_2O_3	2	40	-0.8	0.8	36	This work
IZO	3.5	350	1.2	5	3.8	[4]
ITO	3.5	30	1.2	1	20	[2]
IGZO	8	38	3.5	3	18.3	[9]

Table 1. Benchmark with the best performed RF transistors on BEOL-compatible metal oxide semiconductor alternatives in terms of channel thickness, channel length, biasing voltage, and f_T.